Cite this article
Ganal A, Reul O and Jacobsz SW (2025)
Centrifuge tests on the consolidation behaviour of foundations under alternating loads.
International Journal of Physical Modelling in Geotechnics **25(1)**: 49–65,
https://doi.org/10.1680/jphmg.24.00004

Research Article
Paper 2400004
Received 16/01/2024;
Accepted 10/09/2024;
First published online 20/09/2024

International Journal of Physical Modelling in Geotechnics

Centrifuge tests on the consolidation behaviour of foundations under alternating loads

Aljoscha Ganal Dr-Ing
Department of Geotechnical Engineering, Faculty of Civil and Environmental Engineering, University of Kassel, Kassel, Germany (Orcid:0009-0009-1536-8100) (corresponding author: a.ganal@uni-kassel.de)

Oliver Reul Prof Dr-Ing
Department of Geotechnical Engineering, Faculty of Civil and Environmental Engineering, University of Kassel, Kassel, Germany (Orcid:0000-0002-1700-6324)

S. W. Jacobsz Prof Dr-Ing
Department of Civil Engineering, University of Pretoria, Pretoria, South Africa (Orcid:0000-0002-7439-2276)

This paper presents the results from centrifuge tests on raft foundations and piled rafts in overconsolidated kaolin clay carried out in a beam centrifuge at the University of Pretoria. The foundations were subjected to unloading and reloading phases as well as to multiple consecutive groundwater drawdowns, simulating typical loading scenarios of structures in an urban environment. In order to investigate the time-dependent load-deformation behaviour of foundations, the settlement of the foundations, the pore water pressures at different depths and the axial strains in the piles, from which pile resistances were then derived, were measured continuously. In the tests, repeated groundwater drawdowns resulted in a settlement accumulation, with the increase in settlements decreasing with each repetition. The pile position within the pile group was found to have a major impact on the mobilised pile resistance. The position, however, became less significant as the load level increased. Furthermore, insights were gained concerning the load distribution within piled rafts during consolidation.

Keywords: alternate loading/centrifuge modelling/clay/consolidation/creep/groundwater drawdown/load transfer/overconsolidation/piled raft

Notation

C_U	coefficient of uniformity
d_{CPT}	CPT probe diameter
d_p	pile diameter
L_p	pile length
N	scaling factor in the centrifuge
N_{kt}	correction factor to estimate the undrained shear strength
P	load applied on the raft
p	uniform stress applied on the raft
q_c	cone tip resistance in the cone penetrometer tests
R_{avg}	average pile resistance of a pile in the piled raft
R_b	pile base resistance
$R_{b,avg}$	average pile base resistances
R_{centre}	average pile resistances of a centre pile
R_{corner}	average pile resistances of a corner pile
R_{edge}	average pile resistances of a edge pile
R_{pile}	pile resistance
R_{raft}	raft resistance
R_s	pile shaft resistance
$R_{s,avg}$	average pile shaft resistances
R_{tot}	total resistance of the foundation
s	settlement
s_{creep}	creep settlement
s_{norm}	normalised settlement
s_R	average settlement of the foundation
s_S	average settlement of the soil
s_u	undrained shear strength
t_{EOP}	end of primary consolidation
t_p	wall thickness of the pile
t_r	thickness of the raft
u	pore water pressure
z	depth
α_b	share of the pile base resistance on the pile resistance
α_p	normalised pile resistance
α_{pr}	piled raft coefficient
σ_v	vertical stress of the soil at 80g
Δd_{GW}	change in the groundwater level
Δp_{phase}	stress applied within one loading phase
Δs_R	change in the average settlement of the foundation
Δt	time of one groundwater drawdown
Δu	excess pore water pressure
$\sum R_{pile}$	sum of all pile resistances in the piled raft

1. Introduction

When planning the reuse of existing foundations, the previous loading history of the foundation and subsoil due to building load and demolition, if present, must be taken into account, as it can have a major influence on the future bearing behaviour of an

existing foundation. In cities such as Frankfurt am Main and London, where the subsoil conditions are characterised by fine-grained soils, the time-dependent material behaviour must be considered as well. The prediction of the time-dependent load-settlement behaviour of foundations in clayey soils is particularly important when existing and new foundation elements are to be integrated, which is becoming increasingly important, especially in inner-city areas (Butcher *et al*., 2006).

In addition to the time-dependent deformation behaviour of the soil due to the construction itself caused by consolidation processes and the time-dependent material behaviour (creep), the long-term deformation behaviour of foundations is also influenced by changing building loads resulting from demolition and reconstruction phases as well as by construction activities in the surrounding area. In particular, the influence of neighbouring groundwater drawdown has to be considered in this context, resulting in changes in uplift and the effective stresses in the subsoil.

Furthermore, settlements continue to occur long after the buildings have been completed (Ganal and Reul, 2023; Hooper, 1973; Reul, 2000; Tang *et al*., 2014; Yamashita, 2012) due to the slow dissipation of the excess pore water pressure (PWP) generated during the construction period or/and due to creep. The dissipation of excess PWP changes the effective stresses in the ground, causes deformation, and changes the load sharing between the raft and the piles in the case of a piled raft (e.g. Cooke *et al*., 1981; Franke and Lutz, 1994; Reul, 2002). Therefore, when designing foundations in clayey soils, the behaviour of the foundation needs to be predicted throughout its entire service life, including construction and (partial) demolition, as well as consolidation and creep phases.

In a recent research project (Ganal, 2024), extensive investigations were carried out on the long-term deformation behaviour of foundations in overconsolidated (oc) clay. In this context, measurements on high-rise foundations in Frankfurt am Main extending over several decades were evaluated and an extensive laboratory test programme, centrifuge tests and numerical studies were conducted.

This paper summarises the results of the centrifuge test on raft foundations and piled rafts in oc clay carried out in the scope of this research project. The bearing behaviour of piled rafts is characterised by the interaction between the piles and the raft. Individual pile resistances depend on the positioning within the pile group (e.g. Reul, 2004). Under practical loading conditions, the piles in a piled raft typically do not attain their ultimate bearing capacity (Reul, 2004). As a result, deformation criteria, specifically the serviceability limit state, rather than the ultimate limit state bearing capacity, govern the design of piled rafts (Reul and Randolph, 2004). These aspects were considered in defining the boundary conditions for the experiments, also considering parameters such as pile spacing and the load levels investigated.

2. Test programme

The centrifuge tests described in this paper were carried out in the beam centrifuge at the University of Pretoria with a platform radius of 3 m capable of accelerating 1500 kg to an acceleration of 100***g*** (Jacobsz *et al*., 2014).

The test programme comprised six centrifuge tests on vertically loaded piled rafts (PR) and raft foundations (R) under varying groundwater levels (Loading scheme A) and alternating vertical loads (Loading scheme B), respectively (Table 1). The aim was to simulate typical loading scenarios of structures in an urban environment. Centrifuge test PR-B and R-B were repeated to investigate the reproducibility of the results. The results of test PR-B-I were already published in Ganal *et al*. (2022). The present publication focuses mainly on the experiments PR-A and PR-B on piled rafts.

All tests were executed at a nominal centrifugal acceleration of 80***g***. All results presented throughout the work are at model scale and can be converted to prototype scale applying the scaling factors after Taylor (1995).

2.1 Experimental set-up

The test set-ups for the two foundation configurations, that is raft foundation and piled raft, are basically identical, with the piles being the only difference. The general test layout for the case of the piled raft foundation is shown as a cross-section in Figure 1(a) and as a ground plan in Figure 1(b). The raft, a square, 150 mm × 150 mm aluminium plate (thickness $t_r = 16$ mm), is located in the centre of a strong box with a plan area of 400 mm × 600 mm. Applying the definition by Horikoshi and Randolph (1997), the raft–soil stiffness ratio can be established as $K_{rs} \approx 100$, indicating an essentially rigid raft. Beneath the raft, 16 piles were installed in a 4 × 4 grid (spacing of $d_{sp} = 4 \cdot d_p$). The model piles comprised smooth aluminium tubes of diameter $d_p = 10$ mm, length $L_p = 150$ mm and wall thickness $t_p = 1.25$ mm

Table 1. Test programme

Test	PR-A	PR-B	R-A	R-B	PR-B-I	R-B-I
Foundation type	Piled raft	Piled raft	Raft foundation	Raft foundation	Piled raft	Raft foundation
Loading scheme	A	B	A	B	B	B

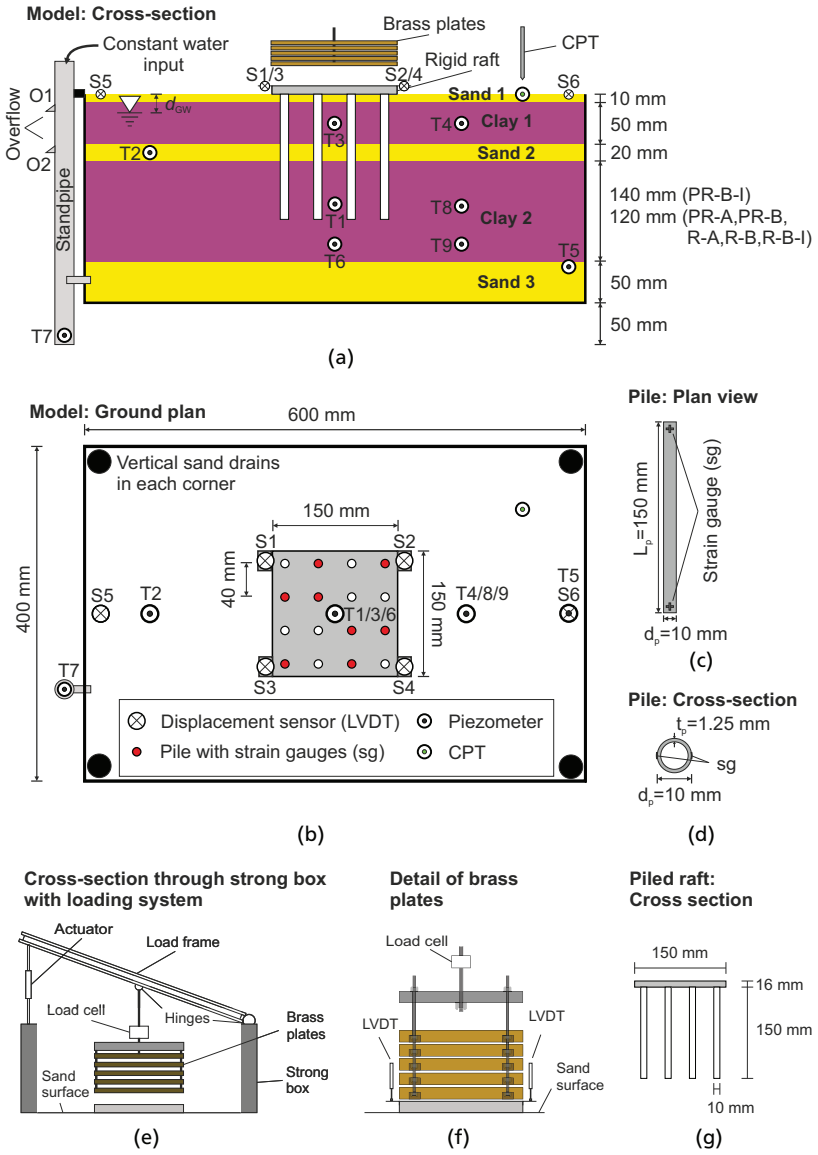

Figure 1. Test layout

(Figures 1(c) and 1(d)). The pile heads fitted into recesses in the raft, giving a rigid connection. Model and prototype dimensions are summarised in Table 2. The prototype raft thickness was defined such that the bending stiffness of a concrete cross-section corresponds to that of the aluminium cross-section of the model.

To apply the load, five brass plates were lowered separately onto the raft with the help of a linear actuator (Figures 1(e) and 1(f)). To monitor the load actually applied to the raft, the weight of the brass plates carried by the load frame was measured by a load cell, that is the load P applied on the raft is the difference between the weight of all brass plates and the force measured by the load cell.

The groundwater level was controlled using a standpipe that was provided with a constant water flow and two overflows (O1 and O2) (Figure 1(a)). O1 was always open and therefore specified the initial water level. In the event of a groundwater lowering, O2 was opened using a valve. To ensure equalisation of water heads in the different soil layers, vertical sand drains were installed in the four corners of the box.

The soil stratigraphy in the centrifuge tests comprised 10 mm of sand (Sand 1) to ensure a proper contact between raft and soil, followed by 50 mm oc clay (Clay 1), 20 mm of sand (Sand 1) and 120 mm respectively 140 mm oc clay (Clay 2). A 50 mm thick

Table 2. Model and prototype dimensions of raft and piles

	Parameter		Model		Prototype		
	Material	—	Aluminium		Concrete	Aluminium	—
	Young's modulus	E	70 000	[MPa]	30 000	70 000	[MPa]
	Poisson's ratio	v	0.34	—	0.2	0.34	—
Raft	Thickness	t_r	16	[mm]	1.7	1.28	[m]
	Width	L_r	150	[mm]	12	12	[m]
	Bending stiffness	EI	240	[kPa]	146 800	146 800	[MPa]
Piles	Diameter	d_p	10	[mm]	0.8	0.8	[m]
	Wall thickness	t_p	1.25	[mm]	—	0.1	[m]
	Length	L_p	150	[mm]	12	12	[m]
	Cross-sectional stiffness	EA	2.4	[MPa]	15 080	15 394	[MPa]
	Bending stiffness	EI	0.024	[kPa]	603	962	[MPa]

sand layer (Sand 3) at the base of the strong box, separated from Clay 2 by means of a thin geotextile, served as a drainage layer.

The instrumentation in the tests shown in Figures 1(a)–1(c) included four piezometers in Clay 1 and Clay 2 to monitor the consolidation process and three piezometers located in Sand 2 and Sand 3 and in the standpipe used to control the groundwater level. It should be noted that the indicated piezometer depths may differ from the final position, as they were installed into the clay slurry during model preparation. The exact final positions are documented in Ganal (2024). The piezometers used are high-capacity tensiometers constructed at the University of Pretoria (Jacobsz, 2018), already successfully used in different projects, for example Narainsamy and Jacobsz (2023).

The vertical displacements of the raft were measured with four LVDTs (linear variable differential transformers) (S1–S4). Two more displacement transducers were used to measure the surface displacements (S5 and S6).

Eight piles were equipped with one pair of strain gauges at the pile head and one pair of strain gauges at the pile base to derive the axial load transferred to the piles using the mean axial strain ε_a and the cross-sectional stiffness EA (Figures 1(c) and 1(d)).

The piles equipped with strain gauges were chosen so that at least two piles of each position (corner, edge, centre) were instrumented (Figure 1(b)).

2.2 Model preparation

According to Thaher and Jessberger (1991) and Taylor (1995), the soil can be prepared outside the centrifuge and then reconsolidated in the centrifuge without changing its properties. The aim was to obtain an overconsolidation ratio of $OCR = 2.5$ at the pile bases during centrifuge tests, comparable to the OCR encountered at the pile base of piled rafts in the Frankfurt, Germany (e.g. Ganal, 2024).

During the preparation of the model, layer Sand 3 was placed at the base of the box covered by a thin geotextile. Layer Clay 2 was consolidated from a kaolin slurry with a water content of 100%, initially using weights to gradually apply 12 kPa. To produce an oc sample, a stress of $p = 246$ kPa was subsequently applied in several steps to the surface using a hydraulic press. During the consolidation, both the PWP and the settlement of the sample were monitored. The load was increased once the excess PWP had dissipated and the settlements completed. After the consolidation process was completed, Sand 2 was rained at an estimated dry unit weight of $\gamma_d = 14.6\,\mathrm{kN/m^3}$ leading to a saturated unit weight of $\gamma_{sat} \approx 18.6\,\mathrm{kN/m^3}$. The procedure was then repeated for layers Clay 1 and Sand 1. The OCR profile from this temporary preloading is shown in Figure 2 for a model at 80***g***.

2.3 Soil properties

The strength characterisation of the samples was undertaken immediately after each centrifuge test by means of cone penetrometer tests (CPTs) with $d_{CPT} = 8$ mm (Figure 3). The CPTs were carried out at 80***g*** after a short stop of the centrifuge to remove the load-application actuator. Assuming a correction factor of

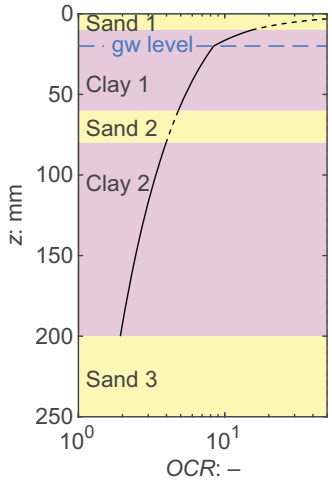

Figure 2. OCR profile at 80***g***

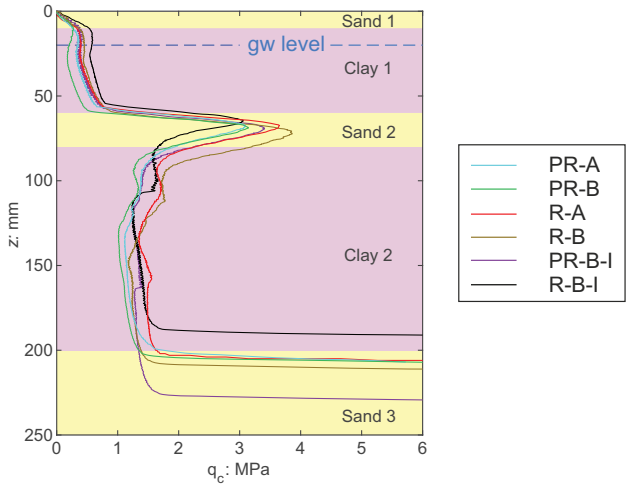

Figure 3. CPT profiles of the six tests

$N_{kt} = 15$, the undrained shear strength s_u can be estimated according to Equation 1. The average values for the individual layers, summarised in Table 3, were $s_u \approx 31$ kPa in Clay 1 and $s_u \approx 78$ kPa in Clay 2.

1. $$s_u = (q_c - \sigma_v)/N_{kt}$$

The properties of the kaolin clay, classified as a medium plasticity silt (Ganal (2024), and the sand are listed in Tables 4 and 5, respectively. The particle size distributions for both sand and kaolin clay are presented in Figure 4.

2.4 General testing procedure

After the model soil profile had been prepared, either the raft was placed on the sand and levelled or the piled raft was jacked into the soil as a group at 1***g*** using a press (Ganal, 2024). After the piled raft was jacked, it took about 12 h to start the tests (spin-up phase). It is assumed that the behaviour of 'pre-jacked' piles is comparable to bored piles in the field (Li *et al.*, 2010). Water was only added to the model shortly before starting the centrifuge to prevent excessive swelling of the kaolin. To keep the groundwater level constant throughout the test, water was added continuously by way of a standpipe connected to the strong box, with the overflow O1 ensuring the desired height (Figures 1(a) and 1(b)). Following this, the foundation was loaded by means of the brass plates lowered consecutively onto the raft to $p \approx 275$ kPa. After a consolidation phase, an unloading and reloading of the foundation or a groundwater drawdown was performed, followed again by a consolidation phase (Figures 5 and 11). During the consolidation phase, creep occurs simultaneously. However, assuming a scaling factor of $N_{t,c} = 1$ (Taylor, 1995) for creep and considering that the oc kaolin has a rather low viscosity, creep is assumed to be of minor importance compared with consolidation.

Table 4. Properties of the kaolin clay

Parameter			
Saturated unit weight	γ_{sat}	[kN/m^3]	18.2
Dry unit weight	γ_d	[kN/m^3]	13.0
Plastic limit	PL	[%]	36
Liquid limit	LL	[%]	47
Percentage of particles $d <$ 0.002 mm	—	[%]	31
Activity index	I_A	—	0.35
Critical friction angle	φ_c	[°]	28.6
Compression index	C_c	—	0.129
Swelling index	C_s	—	0.030[a]
Viscosity index	I_v	—	0.012
Constrained modulus	E_s	[MN]	$1.46 + 0.23 \cdot z$
Permeability coefficient	k	[m/s]	$3 \cdot 10^{-10}$

[a]After pre-consolidation stress of $\sigma_{v,max} = 1600$ kPa
Note: $z \triangleq$ depth below ground surface [m]

Table 5. Properties of the sand

Parameter			
Saturated unit weight	γ_{sat}	[kN/m^3]	18.5
Dry unit weight	γ_d	[kN/m^3]	14.6
Mean grain size	d_{10}	[mm]	0.283
Effective grain size	d_{50}	[mm]	0.138
Critical friction angle	φ_c	[°]	33
Coefficient of uniformity	C_U	—	2.32

3. Results

3.1 General remarks

This publication discusses the results of the two tests on piled rafts labelled PR-A and PR-B. The data from the tests on the

Table 3. Average undrained shear strength and height of the clay layers

Layer	Parameter			PR-A	PR-B	R-A	R-B	PR-B-I	R-B-I
Clay 1	Undrained shear strength	s_u	[kPa]	26	16	30	32	29	43
	Height	h_{clay}	[mm]	46	50	44	46	46	46
Clay 2	Undrained shear strength	s_u	[kPa]	74	68	82	83	75	87
	Height	h_{clay}	[mm]	112	121	115	119	132	111

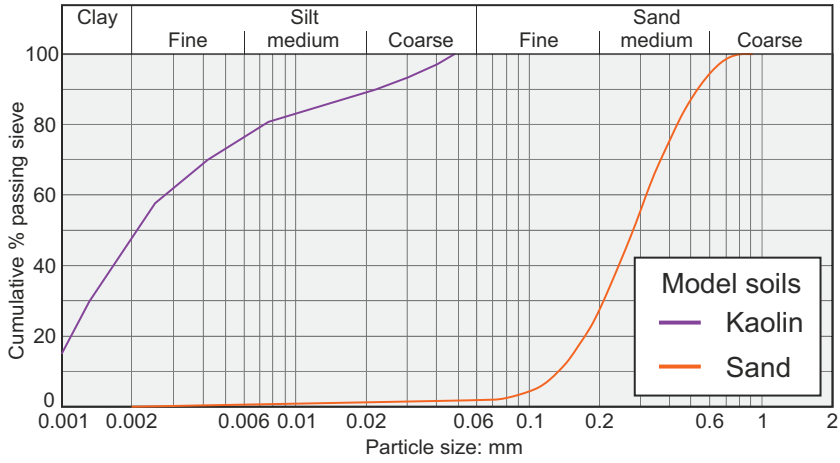

Figure 4. Grain size distribution of the model soils

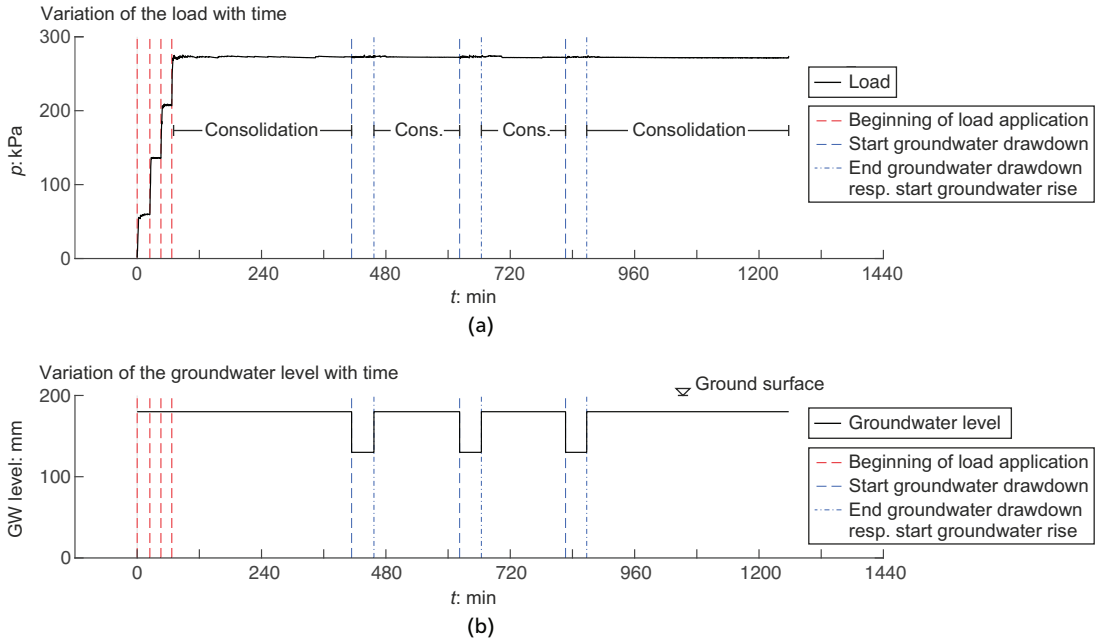

Figure 5. Test PR-A: variation of load and groundwater level with time

raft foundations R-A and R-B, as well as the test data of the repeat tests PR-B-I and R-B-I, are compiled in Ganal (2024). Both repeat tests showed qualitatively the same results as the corresponding tests PR-B and R-B. Test PR-B-I was presented by Ganal *et al*. (2022).

The settlement of the foundation s_R is the mean settlement of all four LVDTs on the foundation, whereas the settlement of the surrounding soil s_S is the mean settlement of the two LVDTs located on the soil surface.

The total resistance R_{tot} mobilised by the foundation equals the measured load applied to the foundation (i.e. the dead weight of the raft is not taken into account):

2. $R_{tot} = P$

The resistance of a pile type (i.e. corner, edge or centre) is the average value of the monitored instrumented piles at that

position (e.g. Figure 14). The average mobilised pile resistance R_{avg} then results from the weighted average of the mobilised resistances of the individual pile positions:

$$3. \quad R_{avg} = \frac{4 \cdot R_{corner} + 8 \cdot R_{edge} + 4 \cdot R_{centre}}{16}$$

The sum of all mobilised pile resistances is then:

$$4. \quad \sum R_{pile} = 16 \cdot R_{avg}$$

The raft resistance R_{raft} was calculated as the difference between the total resistance R_{tot} and the sum of all pile resistances $\sum R_{pile}$:

$$5. \quad R_{raft} = R_{tot} - \sum R_{pile}$$

The pile load measured with the upper pair of strain gauges is taken equivalent to the mobilised total resistance of the pile R_{pile}, whereas the pile load measured with the bottom pair of strain gauges corresponds to the mobilised base resistance R_b. The mobilised shaft resistance R_s is then:

$$6. \quad R_s = R_{pile} - R_b$$

The average pile shaft resistances $R_{s,avg}$ and base resistances $R_{b,avg}$ are determined following the same procedure as for R_{avg} (Equation 3).

The piled raft coefficient, α_{pr}, describes the ratio of the sum of all mobilised pile resistances $\sum R_{pile}$ to the total resistance mobilised by the foundation R_{tot}:

$$7. \quad \alpha_{pr} = \frac{\sum R_{pile}}{R_{tot}} = \frac{\sum R_{pile}}{P}$$

The normalised pile resistance is defined as:

$$8. \quad \alpha_p = \frac{\frac{1}{n_p}\sum R_{pile,p}}{\frac{1}{n}\sum R_{pile}}$$

where $\sum R_{pile,p}$ = sum of all pile resistances at position p, n_p = number of piles at position p, $\sum R_{pile}$ = sum of all pile resistances and n = number of piles in the pile group.

The pile shaft coefficient, α_s, describes the ratio of the sum of all pile shaft resistances $\sum R_s$ to the sum of all pile resistances $\sum R_{pile}$:

$$9. \quad \alpha_s = \frac{\sum R_s}{\sum R_{pile}}$$

The end of the primary consolidation t_{EOP} is defined by the change of the normalised excess PWP $\Delta u/\Delta p_{phase}$ during the consolidation being less than 1% in 30 min:

$$10. \quad \left(\frac{\Delta u(t_{EOP}) - \Delta u(t_{EOP} - 30\,\text{min})}{\Delta p_{phase}}\right) < 0.01$$

3.2 Spin-up

After spin-up, before starting the loading sequence, the model soil profiles were allowed to consolidate under their weight while monitoring the development of settlements and excess PWP dissipation, which took approximately 2–4 h depending on the test (Ganal, 2024). Once the PWPs had dissipated and the settlements stabilised, the loading sequence was initialised. As expected, the raft foundations experience larger settlements (S1–S4) than the surrounding soil surface (S5 and S6) during spin-up due to their own weight. In contrast, the piled rafts experience smaller settlements than the soil surface, which may result in a loss of contact between the raft and the soil. This may have an impact on the foundation behaviour during the first loading phase, until full contact is established again.

In the remainder of this paper, all results presented refer to the start of the main loading sequence ($t_0 = 0$ min), that is to the end of the consolidation process resulting from the spin-up. Consequently, all settlements and resistances are zeroed at the beginning of the main loading sequence.

3.3 Piled raft: test PR-A

3.3.1 Load sequence

Figure 5(a) shows the development of the load on the piled raft due to the brass plates being successively lowered onto the raft. After the weight of the fourth brass plate was applied, they were kept on the foundation until the end of the test. During the test, the groundwater level was lowered three times for $\Delta t = 41$ min by $\Delta d_{GW} = 50$ mm due to the opening of the overflow O2 on the standpipe (Figures 1(a) and 1(b)). Figure 5(b) shows the variation of the water level in the standpipe, which, for simplicity, is assumed to be identical to the groundwater level, with time.

3.3.2 Settlements

The variation of settlements with time is plotted in Figure 6 for all six displacement transducers. While the sensors S5 and S6 located on the soil surface show more or less identical settlements, the other sensors placed on the raft indicate relatively large differential settlements. In contrast to spin-up, the two sensors S5 and S6 show only minor settlements during load application, which means that the influence of the strong box can be considered small. Although the load increments amount to $\Delta p_{phase} = 68\,\text{kPa}$ in each loading phase, the increase in settlement became significantly larger as the load increased. After the fourth loading phase, and following consolidation at $t = 414\,\text{min}$, the average settlements of the piled raft amount to $s_R = 7.6\,\text{mm}$. Considering the development of the PWP u (Section 3.3.3), the consolidation is completed at $t_{EOP} = 210\,\text{min}$ (Equation 10). The following increase of settlement of $\Delta s_R \approx 0.2$ mm up to the first lowering of the groundwater may thus be assigned to creep, although it is acknowledged that when considering a scaling factor of $N_{t,c} = 1$ (Taylor, 1995) the time to develop such creep settlements is rather short. During the three groundwater drawdown events, considerable settlements occur, which become clearly less with repeated drawdown despite the same drawdown magnitude of $\Delta d_{GW} = 50\,\text{mm}$. The settlements increase more or less uniformly for the entire piled raft and amount to $\Delta s_R = \{0.60, 0.25, 0.15\}$ mm, respectively, for the three groundwater drawdown events, whereas the subsequent groundwater rising causes barely any heave.

3.3.3 Pore water pressures

Figure 7 shows the variation in PWPs with time for all piezometers except T2 (Sand 2) and T9 (Clay 2), which proved not functional.

The piezometers T5 (Sand 2) and T7 (standpipe) basically indicate the hydrostatic water pressure at their respective depths. Both show no reaction to the application of the load, whereas they react immediately to the lowering or rising of the groundwater level due

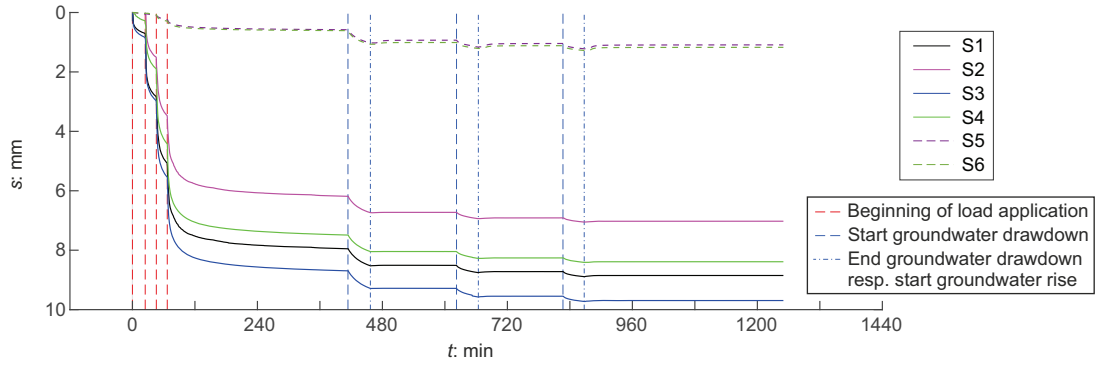

Figure 6. Test PR-A: variation of settlements with time

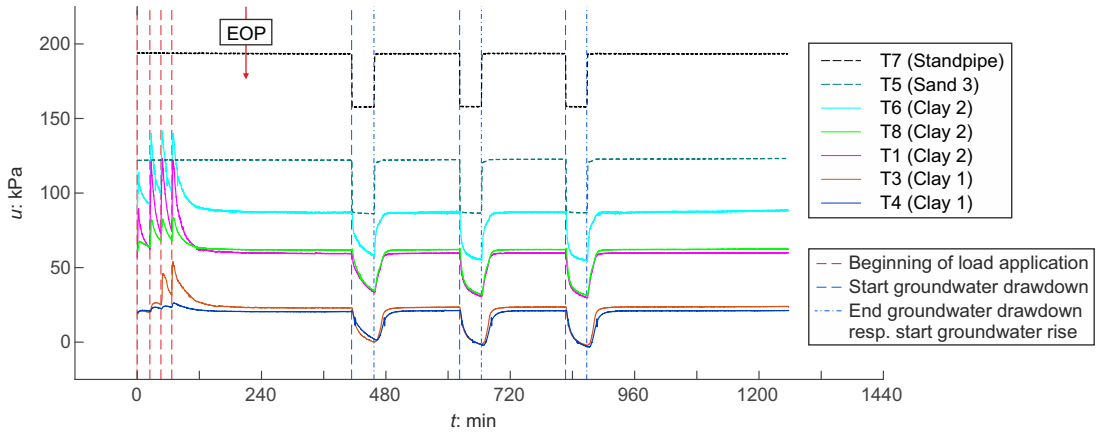

Figure 7. Test PR-A: variation of pore water pressures with time

to their location in the standpipe and the high permeable sand, respectively.

In contrast, the load application is clearly visible in all piezometers embedded in the two clay layers. During each loading phase, the PWP continues to build up to a maximum $\Delta u \approx \Delta p_{phase}$ (T1, T6). When comparing piezometers installed at the same depth (T1/T8 and T3/T4), the excess PWP is significantly higher for piezometers located closer to the loaded raft, as would be expected. Similarly, piezometer T1, which is located above T6, shows slightly higher excess PWPs than the latter.

3.3.4 Pile resistances

The variation of the average pile resistance with time for the different pile positions in the group is shown in Figure 8(a). Figure 8(b) then shows the variation of the normalised pile resistances for the different pile position with time. The pile resistance was observed to increase from centre piles to edge piles to corner piles. However, as the load level increases, the position of the pile within the group becomes less significant. The share of the edge pile remains almost constant over the entire period. During the change in groundwater level, no modification of the load transfer seems to occur within the pile positions of the group.

Figure 9(a) shows variation of the average pile shaft resistance $R_{s,avg}$, the average pile base resistance $R_{b,avg}$ and the average pile resistance R_{avg} with time. During a groundwater drawdown, there is an increase in pile resistance. With the following groundwater rise, the pile resistances return to their initial level.

In Figure 9(b), the share of pile shaft resistance α_s is plotted. As can be expected for piles in a relatively homogenous soil, the shaft resistance is responsible for the major share of the pile resistance. Furthermore, a decrease of α_s with increasing load level can be observed. It becomes apparent that the increase in pile resistance during groundwater lowering is almost entirely due to the increase in pile base resistance; thus, the share of pile shaft resistance α_s decreases. With the following groundwater rise, α_s increases compared with the value before the lowering, approaching its initial value again as time passes.

3.3.5 System resistances

The variation of total resistance R_{tot}, raft resistance R_{raft} and sum of all pile resistances $\sum R_{pile}$ with time is documented in Figure 10(a), whereas the piled raft coefficient α_{pr} is plotted in Figure 10(b).

The measurements confirm previous findings (e.g. Reul, 2004) that the load share between piles and raft is not constant for a certain piled raft configuration, but generally decreases with increasing load level. During the centrifuge test, the piled raft coefficient decreased from $\alpha_{pr} = 1.00$ (phase 1) to $\alpha_{pr} = 0.84$ (phase 2) to

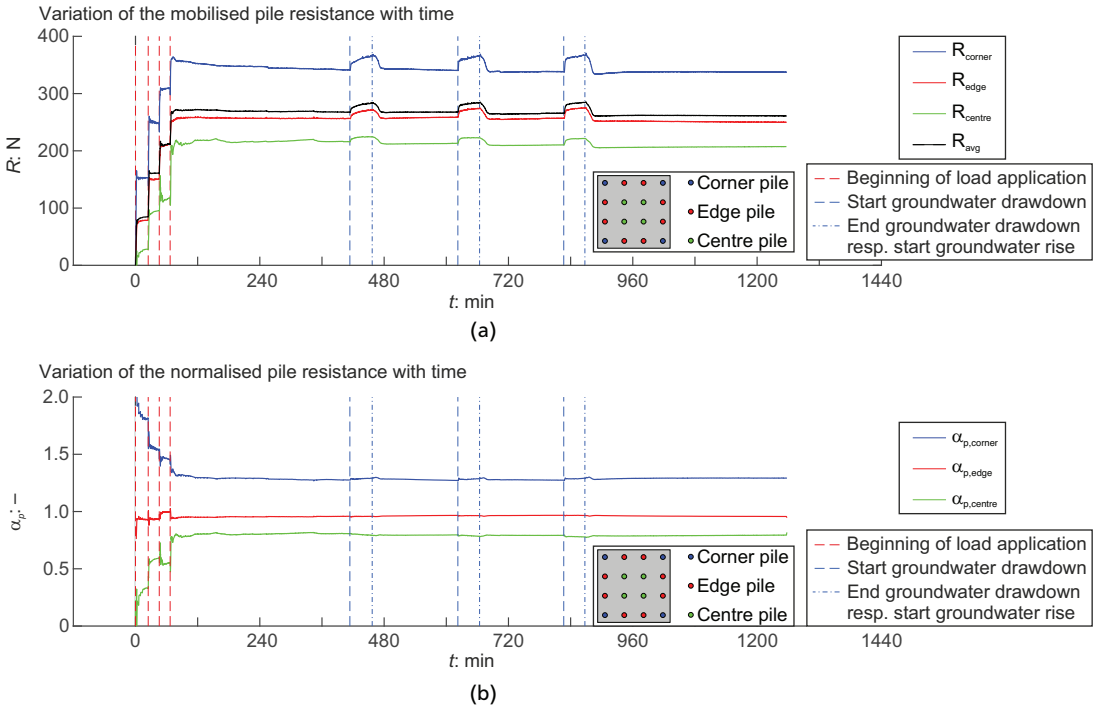

Figure 8. Test PR-A: variation of the mobilised and normalised pile resistance with time

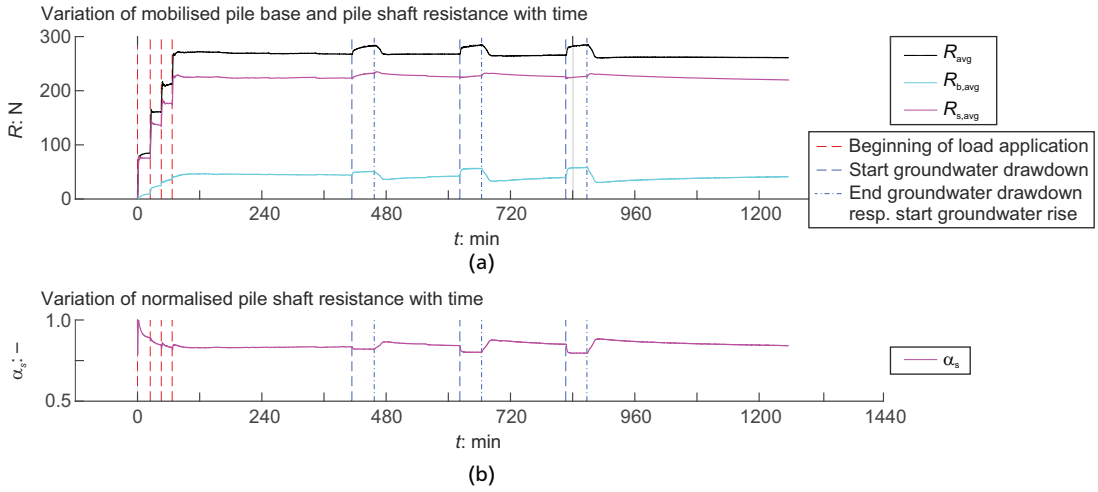

Figure 9. Test PR-A: contribution of pile base resistance and pile shaft resistance

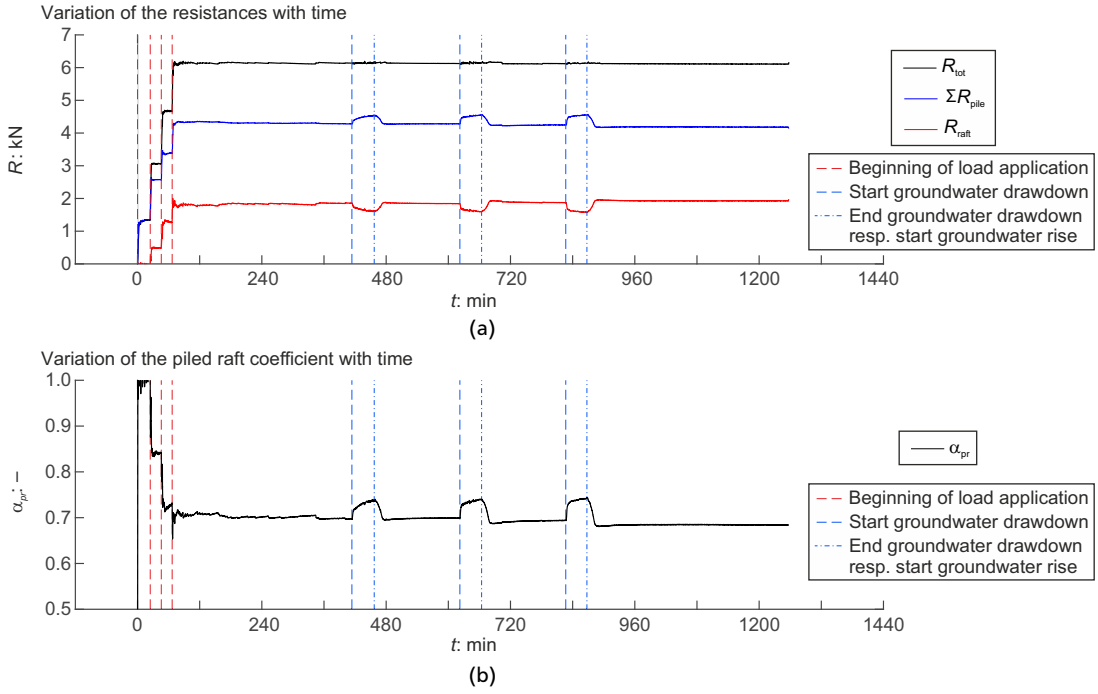

Figure 10. Test PR-A: variation of total resistance, raft resistance, sum of all pile resistances and piled raft coefficient with time

$\alpha_{pr} = 0.70$ (phase 4). However, the piled raft coefficient of $\alpha_{pr} = 1.00$ in phase 1 indicates that probably no full contact was present between the raft and the soil during the initial loading phase and, thus, all loads are carried by the piles.

During a loading phase, that is after the load had been applied and held constant for a period of time, the piled raft coefficient increased. It becomes more pronounced as the α_{pr} becomes smaller, that is more load is transferred by way of the raft and resulting in higher excess PWPs beneath the raft. In phase 4, the piled raft coefficient increased from $\alpha_{pr} = 0.65$ immediately after the load had been applied within approximately 20 min to $\alpha_{pr} = 0.70$. The increase in pile resistance during groundwater lowering, with the overall resistance remaining the same, results in a higher piled raft coefficient

during those periods. However, after the groundwater level returned to its initial value, the piled raft coefficient was slightly lower than before the drawdown. Over all three cycles, the piled raft coefficient decreases from $\alpha_{pr} = 0.70$ before the first groundwater drawdown to $\alpha_{pr} = 0.68$ after the last groundwater rising.

3.4 Pile raft: test PR-B

3.4.1 Load sequence

Figure 11 shows the variation of the loading on the piled raft with time for the test PR-B with the groundwater level kept constant. Due to the announcement of an unscheduled power interruption after the test had already been running for 3 h, the consolidation phases were shortened compared with test PR-A.

3.4.2 Settlements

The variation of settlements with time is plotted in Figure 12. As in test PR-A, the sensors S5 and S6 located on the soil surface close to the strong box walls show almost no displacements. The sensors S1–S4 placed on the raft indicate relatively large differential settlements, increasing from loading phase 2 onwards. Although the loading increments remain the same, the increase in settlement became generally larger as the load increased, with loading phase 2 being an outlier, showing the most significant increase of settlements. At $t = 345$ min, after the fourth loading phase and the following consolidation phase, the average settlements of the piled raft amount to $s_R = 9.0$ mm. The consolidation is completed after $t_{EOP} \approx 210$ min (Equation 10) so that the following small increase of settlements of $\Delta s_R \approx 0.15$ mm may be assigned to creep settlements. The unloading caused only limited heave, which was completely reversed during the following reloading. The fifth loading phase again resulted in a larger increase in settlement, with an average $s_R = 10.7$ mm at the end of the test. However, due to the unscheduled stop of the experiment, it can be assumed that the settlements had not reached their final values yet.

3.4.3 Pore water pressures

Figure 13 shows the variation of PWPs with time for all piezometers except T3 (Clay 1), which proved not functional. Piezometer T1 stopped working after the fourth loading phase.

The piezometers T2, T5 and T7 show the hydrostatic water pressure at their respective depths. However, T5 and T7 show no

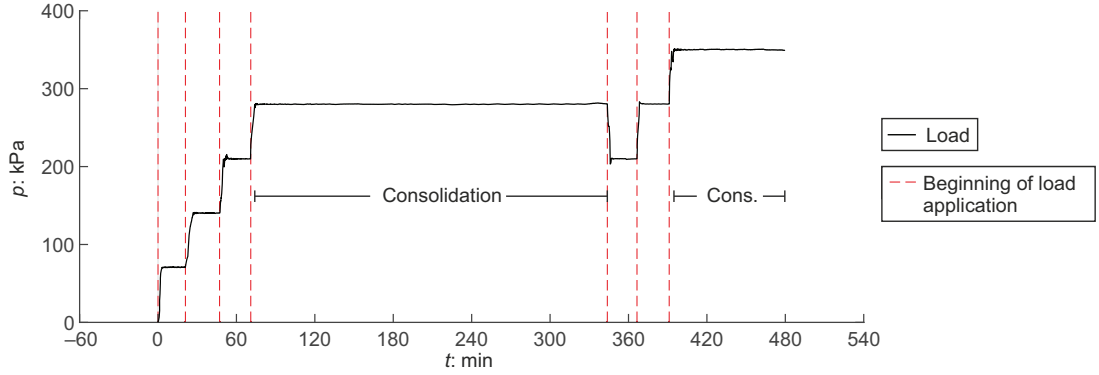

Figure 11. Test PR-B: variation of load with time

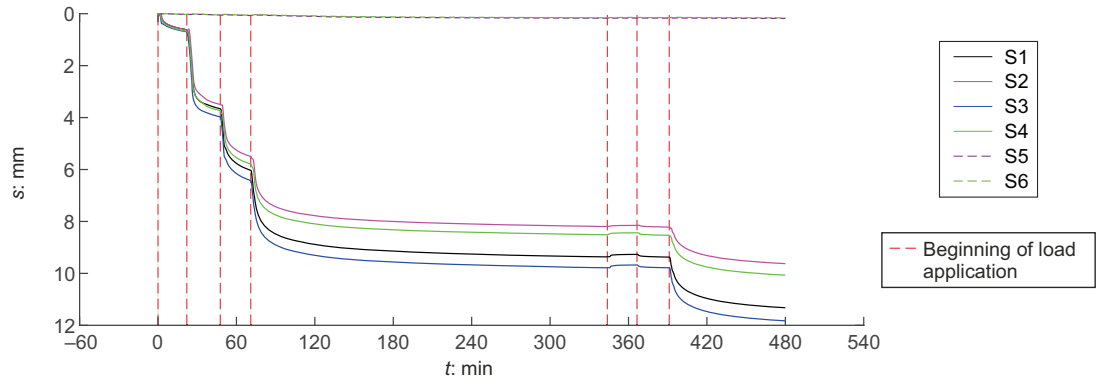

Figure 12. Test PR-B: variation of settlements with time

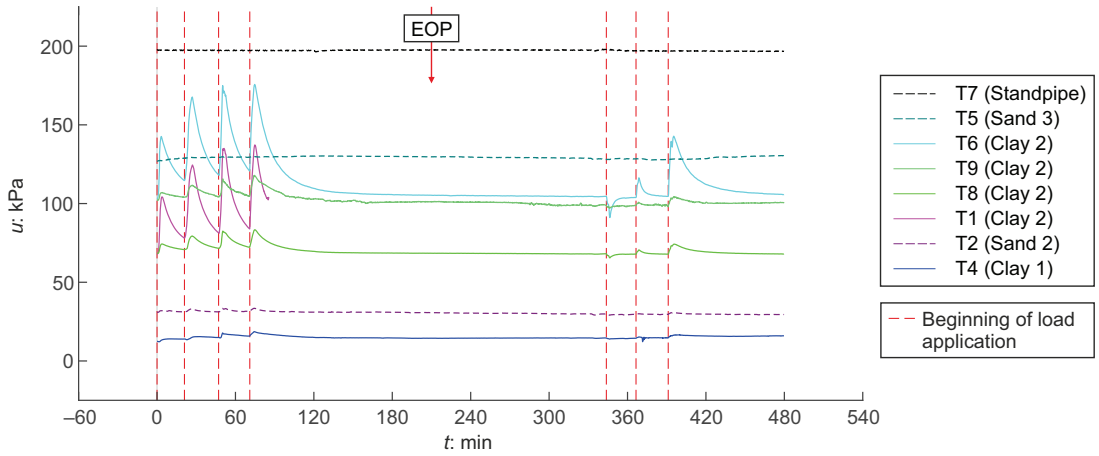

Figure 13. Test PR-B: variation of pore water pressures with time

reaction to the load application and T2 shows limited response, possibly because it was partially embedded in Clay 1.

For the piezometers embedded in the two clay layers, a response to the load application can be seen, with similar effects as described for test PR-A. The excess PWPs during reloading have approximately the same magnitude as the negative excess PWPs during unloading, whereas the subsequent fifth loading phase again leads to a strong increase of excess PWPs.

3.4.4 Pile resistances

The variation of the average pile resistance is shown in Figure 14(a) together with the pile resistances, which increase from centre piles to edge piles to corner piles. However, as observed for test PR-A, the position of the pile within the group becomes less significant with the load level increasing (Figure 14(b)).

Figure 15(a) shows the variation of the average pile shaft resistance $R_{s,avg}$, the average pile base resistance $R_{b,avg}$ and the average pile resistance R_{avg} with time. The decrease in the pile resistance due to the unloading is caused by a loss of resistance of both shaft and base resistance. With increasing load level, a decrease of the pile shaft coefficient α_s was found, resulting in $\alpha_s = 0.72$ at the end of the experiment (Figure 15(b)).

3.4.4 System resistances

Figure 16(a) documents the variation of total resistance R_{tot}, raft resistance R_{raft} and sum of all pile resistances $\sum R_{pile}$ with time, whereas the piled raft coefficient α_{pr} is shown in Figure 16(b).

The load share of the piles α_{pr} is found to increase from the first ($\alpha_{pr} = 0.78$) to the second loading phase ($\alpha_{pr} = 0.85$) and then decreases with further loading to $\alpha_{pr} = 0.73$ at the end of the centrifuge test. The unloading results in a strong increase in α_{pr} even though both R_{raft} and $\sum R_{pile}$ decrease.

Except for loading phase 2, the piled raft coefficient increased after the load had been applied and held constant for a period of time as in test PR-A, indicating a load transfer from the raft to the piles. The increase ranges from $\Delta\alpha_{pr} = 0.03$ in loading phase 1 to $\Delta\alpha_{pr} = 0.05$ in loading phases 3 and 4 after approximately 20 min. In loading phase 4, the load share of the piles increases even further, resulting in an increase during the entire consolidation and creep phase from $\alpha_{pr} = 0.69$ to $\alpha_{pr} = 0.76$.

3.5 Comparative evaluation of the tests

3.5.1 Settlements

The load application phases 1–4 and the subsequent consolidation phase followed the same procedure in all six tests. Despite this, the settlements varied for the same foundation type, which is attributed to the varying stiffness of the soil, especially the upper clay layer (Clay 1), as indicated by the CPT profiles (Figure 3) and the average undrained shear strength (Table 3). In addition, some variation in clay layer thickness contributed to the scatter in results. In order to compare the different tests, the normalised settlement s_{norm} is defined as follows:

$$s_{norm} = \frac{s_R}{h' \cdot p/s'_u}$$

with

11.
$$s'_u = \left(\frac{s_{u,clay1}}{d_{raft,clay1}} + \frac{s_{u,clay2}}{d_{raft,clay2}}\right) / \left(\frac{1}{d_{raft,clay1}} + \frac{1}{d_{raft,clay2}}\right)$$

$$h' = \left(\frac{h_{clay1}}{d_{raft,clay1}} + \frac{h_{clay2}}{d_{raft,clay2}}\right) / \left(\frac{1}{d_{raft,clay1}} + \frac{1}{d_{raft,clay2}}\right)$$

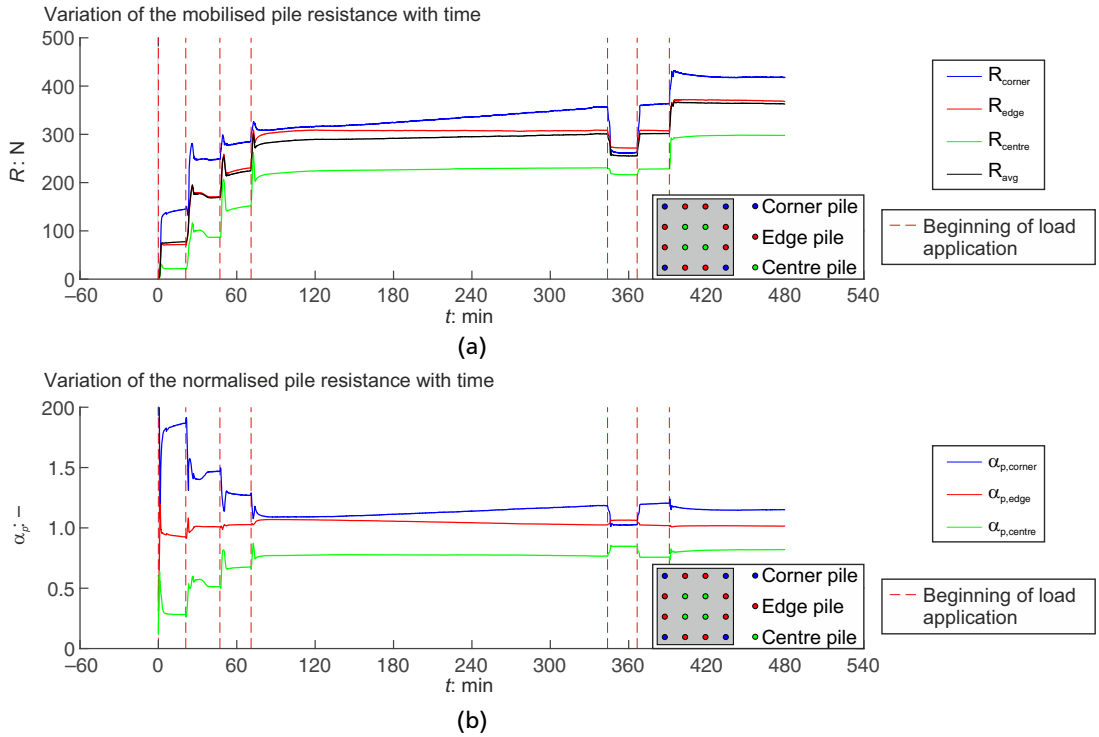

Figure 14. Test PR-B: variation of mobilised and normalised pile resistance with time

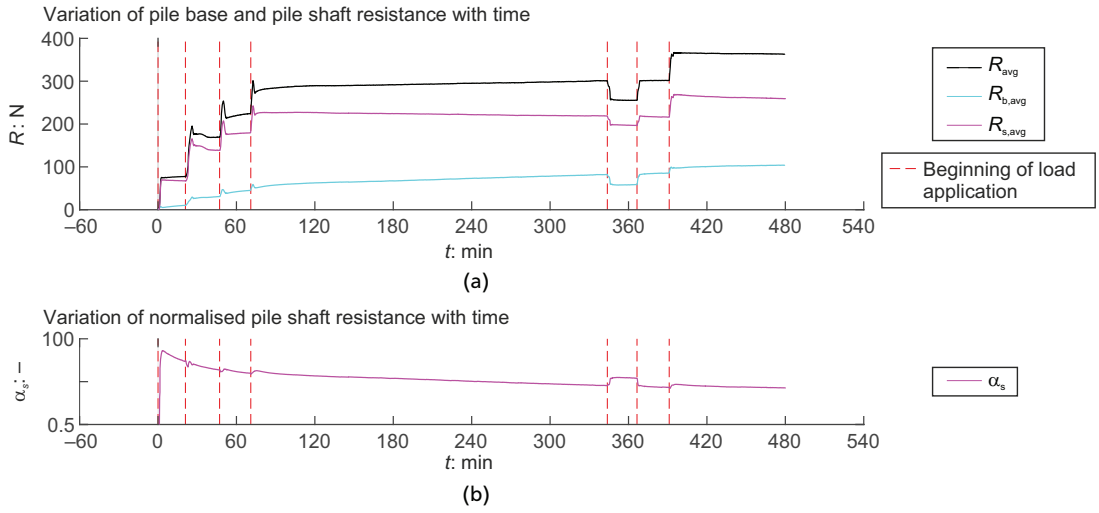

Figure 15. Test PR-B: contribution of pile base resistance and pile shaft resistance

where $s_{u,clay}$ = undrained shear strength for the respective clay layer (Table 3); h_{clay} = height of the respective clay layer (Table 3); $d_{raft,clay}$ = distance from the top edge of the respective clay layer to the bottom edge of the raft.

Figure 17 shows the development of the normalised settlements up to 130 min after the fourth load application. The results of the three tests on piled rafts fall within a relatively narrow band, with the normalised settlements being significantly smaller than for the raft foundations.

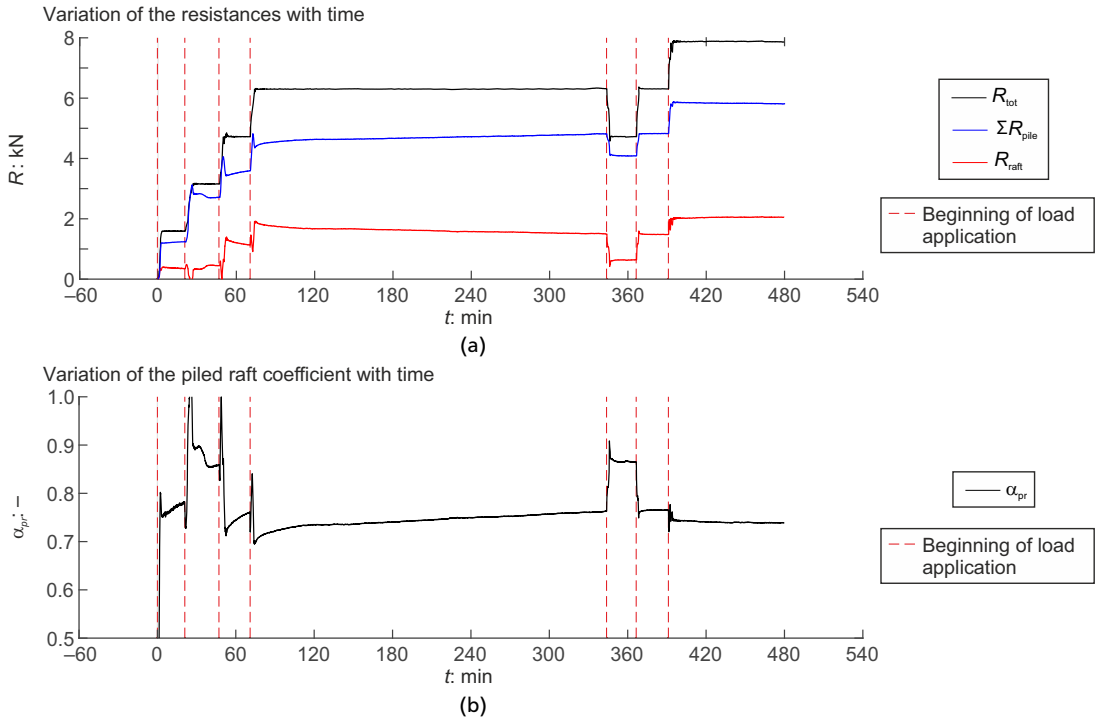

Figure 16. Test PR-B: variation of total resistance, raft resistance, sum of all pile resistances and the resulting piled raft coefficient with time

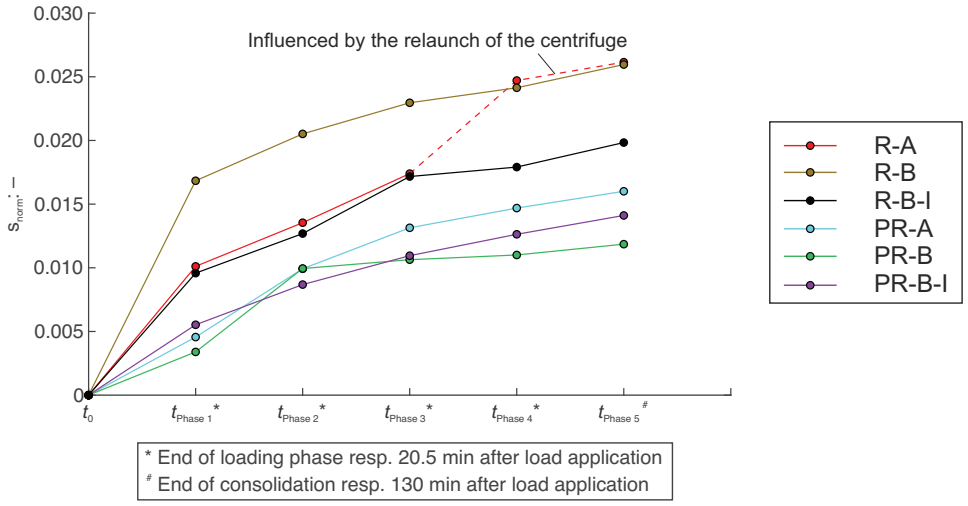

Figure 17. Normalised settlements

Test R-B in particular deviates significantly from the two other tests on raft foundations, which results mainly from the first loading phase. The further development of normalised settlement is then similar to R-A and R-B-I. The small bandwidth of the settlements between the piled rafts indicates a homogenisation of the subsoil by the piles. Excluding test R-B, the raft foundations experience approximately twice (phase 1) to 1.4 times (phase 5) the settlement of the piled rafts.

In the tests PR-A, PR-B, R-A and R-B, the end of consolidation could be determined, which allows settlements of the fourth loading phase to be separated approximately into pure creep and

consolidation settlements, neglecting creep settlements occurring already during consolidation. Creep settlements between $s_{creep} = 0.12$ mm and $s_{creep} = 0.20$ mm were observed, resulting in a contribution to the settlements in phase 4 of approximately 3% for test R-B and 5%–7% for the piled rafts.

As in Rodriguez Rincón *et al*. (2018, 2020) and Tran *et al*. (2012), the present study observed a significant increase in settlements due to a groundwater lowering for both raft foundations and piled rafts. Repeated groundwater drawdowns resulted in a settlement accumulation, with the increase in settlements decreasing with each repetition. Whereas settlements of $\Delta s_R = 0.5$ mm occurred for the raft foundation (test R-A) during the three consecutive drawdowns, slightly higher settlements of $\Delta s_R = 0.9$ mm were observed for the piled raft (test PR-A), corresponding to an increase of 4% and 12%, respectively, related to the end of the consolidation phase 5. This is partly in contrast to Tran *et al*. (2012), where larger settlements for raft foundations than for piled rafts due to a groundwater drawdown were observed. However, in agreement with Tran *et al*. (2012), in the current study the soil experiences less settlement than the piled raft during groundwater drawdown so that, contrary to the observations by Rodriguez Rincón *et al*. (2018) and Rodriguez Rincón *et al*. (2020), full contact of the raft with the underlying sand is maintained.

3.5.2 Pile resistances

In situ measurements (e.g. Sommer *et al*., 1985) and numerical simulations (e.g. Reul, 2004; Ganal, 2024) indicate that the pile resistance of a pile in a piled raft strongly depends on the position of this pile in the pile group. Under working load conditions, the pile resistance can be expected to increase from centre piles to edge piles to corner piles, which is confirmed by the results of the centrifuge tests PR-A, PR-B and PR-B-I (Ganal *et al*., 2022). As the load level increases, however, the position of the pile within the group becomes less significant.

As can be expected for piles in a relatively homogenous soil, the shaft resistance is responsible for the major share of the pile resistance, with the pile shaft coefficient ranging between $\alpha_s = 0.72$ (PR-B) and $\alpha_s = 0.82$ (PR-A) at the end of loading phase 4. However, the α_s decreased with increasing load level in all tests.

3.5.3 System resistances

The development of the piled raft coefficient α_{pr} with the applied load at the end of the respective loading phase is shown in Figure 18. The measurements confirm previous findings (e.g. Reul, 2004) that the load share between piles and raft is not constant for a certain piled raft configuration, but generally decreases with increasing load level after reaching a certain threshold.

During a loading phase, that is after the load had been applied and held constant for a period of time, α_{pr} in most phases increased, with the increase ranging between 1% (phase 2) and 5% (phase 5). This phenomenon is a result of the consolidation process and is also observed in numerical simulations (Ganal, 2024; Reul, 2002).

Similar findings were reported by Hoang and Matsumoto (2020) using small-scale physical modelling to investigate the fundamental mechanisms of the long-term behaviour of vertically loaded piled rafts on saturated clay. The study showed the α_{pr} decreasing with increasing load level, but increasing within one load level during primary consolidation due to an increase in the pile shaft resistance. In contrast, Hoang and Matsumoto (2020) observed no change in α_{pr} due to the settlement during creep.

During an unloading phase, α_{pr} decreased, indicating a load transfer from the piles to the raft.

Both unloading and groundwater lowering resulted in an increase in the load share of the piles, that is an increase in α_{pr}. The increase amounts to approximately 5% during groundwater lowering and approximately 15% during unloading (Figure 18). After reloading and groundwater rise, α_{pr} returned to its previous values.

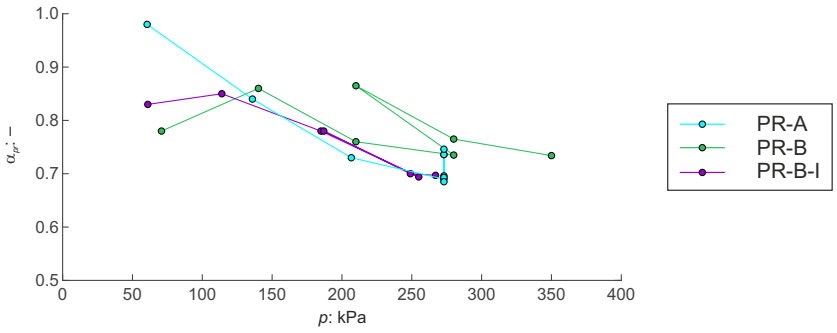

Figure 18. Variation of the piled raft coefficient with load

An increase of the α_{pr} during groundwater lowering was also observed by Rodriguez Rincón *et al*. (2018) and Rodriguez Rincón *et al*. (2020). Tran *et al*. (2012), on the other hand, observed a decrease of α_{pr} by approximately 15% due to a groundwater lowering.

4. Conclusions

The main conclusions drawn from the six centrifuge tests on raft foundations and piled rafts are as follows.

- The narrow bandwidth of the average foundation settlements observed for the different piled rafts as opposite to the raft foundations indicates a homogenisation of the subsoil by the piles.
- Repeated groundwater drawdowns resulted in a settlement accumulation, with the increase in settlements decreasing with each repetition.
- Under working load conditions, the pile resistance can be expected to increase from centre piles to edge piles to corner piles. As the load level increases, however, the position of the pile within the group becomes less significant.
- The load share between piles and raft is not constant for a certain piled raft configuration, but generally decreases with increasing load level after reaching a certain threshold.
- During a loading phase, that is after the load had been applied and held constant for a period of time, the piled raft coefficient generally increases, indicating a load transfer from the raft to the piles as a result of the consolidation process.
- Both unloading and groundwater lowering result in an increase in the piled raft coefficient.

The experimental work presented in this paper forms the basis for further studies on the time-dependent behaviour of foundations where 3D coupled PWP-displacement finite element analyses will be performed with the aim to reproduce the observed effects in order to be able to take them into account in future projects.

Acknowledgements

This research was funded by the German Research Council (DFG) in the framework of project RE 3881/4-1. The financial support from DFG, Germany, is gratefully acknowledged herewith.

REFERENCES

Butcher AP, Powell JJM and Skinner HD (2006) *Reuse of Foundations for Urban Sites: A Best Practice Handbook*. IHS BRE Press, Bracknell.

Cooke RW, Sillett DF, Bryden Smith DW, Smith DWB and Gooch MV (1981) Some observations of the foundation loading and settlement of a multi-storey building on piled raft foundation in London clay. *Proceedings of the Institution of Civil Engineers* **70(3)**: 433–460.

Franke E and Lutz B (1994) Pfahl-Platten-Gründungs-Messungen. *Forschungsabschlussbericht zum Forschungsauftrag Fr 600 - 11/1*.

Ganal A, Reul O and Jacobsz SW (2022) Centrifuge tests on foundations under alternating loads in overconsolidated clay, In *Proc. 10th International Conference on Physical Modelling in Geotechnics (ICPMG)*, *Daejeon, Korea*. Korean Geotechnical Society, Seoul, Korea, vol. 10, pp. 816–819.

Ganal A and Reul O (2023) Back analysis of long-term measurements of a high-rise building founded on a raft foundation in overconsolidated clay. In *Proc. 10th European Conference on Numerical Methods in Geotechnical Engineering (NUMGE), London*, pp. 116.

Ganal A (2024) Time dependent bearing behaviour of foundations subjected to alternate loading in overconsolidated clay. *Schriftenreihe Geotechnik* **30**, https://doi.org/10.17170/kobra-202402209611.

Hoang LT and Matsumoto T (2020) Long-term behavior of piled raft foundation models supported by jacked-in piles on saturated clay. *Soils and Foundations* **60(1)**: 198–217, https://doi.org/10.1016/j.sandf.2020.02.005.

Hooper JA (1973) Observations on the behaviour of a piled-raft foundation on London clay. *Proceedings of the Institution of Civil Engineers* **55(4)**: 855–877.

Horikoshi K and Randolph MF (1997) On the definition of raft-soil stiffness ratio for rectangular rafts. *Géotechnique* **47(5)**: 1055–1061, https://doi.org/10.1680/geot.1997.47.5.1055.

Jacobsz SW, Kearsley E and Kock JHL (2014) The geotechnical centrifuge facility at the University of Pretoria, In *Proc. 8th International Conference on Physical Modelling in Geotechnics (ICPMG)*, January 14-17, 2014, *Perth, Australia*.

Jacobsz SW *et al.* (2018) Low cost tensiometers for geotechnical applications, In *Proc. 9th International Conference on Physical Modelling in Geotechnics (ICPMG)*, July 17–20, 2018, *London, United Kingdom* (McNamara A, Divall S, Goodey R (eds)). CRC Press, an imprint of Taylor and Francis, Boca Raton, FL, pp. 305–310.

Li Z, Haigh SK and Bolton MD (2010) The response of pile groups under cyclic lateral loads. *International Journal of Physical Modelling in Geotechnics* **10(2)**: 47–57, https://doi.org/10.1680/ijpmg.2010.10.2.47.

Narainsamy Y and Jacobsz SW (2023) Evaluating the performance of three sensor types for long-term measurement of suctions in gold tailings. *E3S Web of Conferences* **382**: 16006, https://doi.org/10.1051/e3sconf/202338216006.

Reul O (2000) In-Situ-Messungen Und Numerische Studien Zum Tragverhalten Der Kombinierten Pfahl-Plattengründung. *Mitteilungen Des Institutes Und Der Versuchsanstalt Für Geotechnik Der Technischen Universität Darmstadt 53*.

Reul O (2002) Study of the influence of the consolidation process on the calculated bearing behaviour of a piled raft, In *Proc. 5th European Conference on Numerical Methods in Geotechnical Engineering (NUMGE)*, *Paris, France*.

Reul O (2004) Numerical study of the bearing behavior of piled rafts. *International Journal of Geomechanics* **4(2)**: 59–68, https://doi.org/10.1061/(ASCE)1532-3641(2004)4:2(59).

Reul O and Randolph MF (2004) Design strategies for piled rafts subjected to nonuniform vertical loading. *Journal of Geotechnical and Geoenvironmental Engineering* **130(1)**: 1–13, https://doi.org/10.1061/(ASCE)1090-0241(2004)130:1(1).

Rodriguez Rincón E, Cunha RP, Caicedo B *et al.* (2018) Behaviour of piled raft foundation systems in soft soil with consolidation process, In *Proc. 9th International Conference on Physical Modelling in Geotechnics (ICPMG)*, July 17–20, 2018, *London, United Kingdom* (McNamara A, Divall S, Goodey R (eds)). CRC Press, an imprint of Taylor and Francis, Boca Raton, FL, pp. 1407–1411.

Rodriguez Rincón E, Cunha RP and Caicedo HB (2020) Analysis of settlements in piled raft systems founded in soft soil under

consolidation process. *Canadian Geotechnical Journal* **57(4)**: 537–548, https://doi.org/10.1139/cgj-2018-0702.

Sommer H, Wittmann P and Ripper P (1985) Piled raft foundation of a tall building in Frankfurt clay. In *Proc. 11th ICSMFE in San Francisco* (ISSMGE (ed.)), pp. 2253–2257.

Tang YJ, Pei J and Zhao XH (2014) Design and measurement of piled-raft foundations. *Proceedings of the Institution of Civil Engineers - Geotechnical Engineering* **167(5)**: 461–475, https://doi.org/10.1680/geng.13.00004.

Taylor RN (ed.) (1995) *Geotechnical Centrifuge Technology*. Blackie Academic & Professional, London, New York.

Thaher M and Jessberger HL (1991) The behavior of pile-raft foundations, investigated in centrifuge model tests, In *Proc. International Conference Centrifuge 91, Boulder* (Hon-Yim Ko (ed.)). Balkema [1991], Rotterdam, pp. 225–234.

Tran TV, Teramoto S, Kimura M, Boonyatee T and Vinh LB (2012) Effect of ground subsidence on load sharing and settlement of raft and piled raft foundations. *International Journal of Civil and Environmental Engineering* **6(2)**, https://doi.org/10.5281/zenodo.1074345.

Yamashita K (2012) Field measurements on piled raft foundations in Japan, In *9th Int. Conf. on Testing and Design Methods for Deep Foundations*.

How can you contribute?

To discuss this paper, please email up to 500 words to the editor at support@emerald.com. Your contribution will be forwarded to the author(s) for a reply and, if considered appropriate by the editorial board, it will be published as discussion in a future issue of the journal.

International Journal of Physical Modelling in Geotechnics relies entirely on contributions from the civil engineering profession (and allied disciplines). Information about how to submit your paper online is available at www.icevirtuallibrary.com/page/authors, where you will also find detailed author guidelines.